



Characterization of magnetic properties and microstructures for Co²⁺ ions-doped Ni–Cu–Zn ferrites

Jingkui Zhao¹ · Xiansong Liu¹ · Xucai Kan¹ · Zuhua Chen¹ · Chaocheng Liu¹ · Wei Wang¹ · Qingrong Lv¹ · Jingwen Huang¹ · Mudssir Shazeda¹

Received: 13 February 2020 / Accepted: 20 April 2020 / Published online: 27 April 2020
© Springer Science+Business Media, LLC, part of Springer Nature 2020

Abstract

In this study, novel Ni–Cu–Zn ferrites with the chemical formula $[\text{Ni}_{0.6}\text{Zn}_{0.4}][\text{Cu}_{0.2}\text{Co}_x\text{Fe}_{1.8-x}]\text{O}_4$ ($x=0, 0.05, 0.10, 0.15, 0.20, 0.25$) doped with Co²⁺ ions were designed and manufactured by standard solid-state reaction method. The magnetic properties, surface characteristics, and ion occupancy of ferrites were studied by X-ray powder diffraction (XRD), scanning electron microscopy (SEM), and vibrating sample magnetometer (VSM), and we explained the different mechanisms of the results and the relationship between magnetic properties and microstructures. For the obtained samples, cobalt ions entered the lattice, and all samples were characterized as spinel structures. As the doping amount of Co²⁺ ions increases, the lattice constant and volume of the sample also increases. With an appropriate doping level, Co²⁺ ions-doped Ni–Cu–Zn ferrites can maintain higher saturation magnetization, higher magnetic permeability, and lower hysteresis loss. When $x \leq 0.1$, the saturation magnetization M_s increases significantly as the doping amount of Co²⁺ ions increases, but when $x > 0.1$, the value decreases. The experimental results show that the saturation magnetization value is 118.08 emu/g, the magnetic permeability value is 39.47 H/m, and the hysteresis loss is 1.192 mW/cm³ at an optimum doping amount. Therefore, the sample achieves the best magnetic properties when the doping amount is 0.1.

1 Introduction

Recently, Ni–Cu–Zn ferrites have the widest range of applications and excellent performance in the high frequency range, which are called the most versatile soft magnetic material [1, 2]. Ni–Cu–Zn ferrites are usually used in transformers, inductors, amplifier cores, switching power supplies, etc. Because they have the advantages of high magnetization, high Curie temperature and large volume, and relatively simple manufacturing process [3, 4]. In the application process, large current returns are required to generate electromagnetic induction, which require high saturation magnetization, high magnetic permeability, and low hysteresis loss [5–7]. Therefore, it is valuable to further

research the properties of Ni–Cu–Zn soft magnetic material systematically.

In a study, Shirsath et al. [8] synthesized Dy³⁺ ions-doped Ni–Cu–Zn ferrites by sol–gel method and they disclosed an enhancement in magnetic properties. The spins of Fe³⁺ ions at the A and B sites are parallel and opposite. Adding some appropriate cations to break the balance between them can obtain better magnetic properties. In another study, Li et al. [9] reported on Co²⁺ ions-doped Ni–Zn ferrites and enhanced its magnetic properties. For ferrites, metal ions are distributed in the “A” and “B” sites, metal ions pass through the intermediate oxygen ions, the composition of the bond angle is different, so there are three types of super-exchange, named A–A, B–B, and A–B [10–12]. According to Neel’s molecular field model, the A–B type has the strongest super-exchange effect, the B–B type has the second super-exchange effect, and the A–A type has the weakest super-exchange effect [13]. Much related literature proves that Cu²⁺ and Ni²⁺ ions in Ni_{0.6}Cu_{0.2}Zn_{0.4}Fe_{1.8}O₄ ferrite materials tend to occupy the octahedral position (B-site), Zn²⁺ ions have the characteristics of occupying the A-site, and Fe³⁺ ions tend to occupy A-site and B-site [14–16]. Some suitable cations are used to substitute Fe³⁺ ions, where the soft magnetic

✉ Xiansong Liu
xiansongliu@ahu.edu.cn

✉ Xucai Kan
kanxucai@ahu.edu.cn

¹ Engineering Technology Research Center of Magnetic Materials, School of Physics & Materials Science, Anhui University, 111 Jiulong Road, Hefei 230601, People’s Republic of China

properties will be changed. The purpose of this paper is to study the microstructures and soft magnetic properties of samples after Co^{2+} ions replace Fe^{3+} ions.

In this work, novel Co^{2+} ions-doped Ni–Cu–Zn ferrites with a nominal chemical formula $[\text{Ni}_{0.6}\text{Zn}_{0.4}][\text{Cu}_{0.2}\text{Co}_x\text{Fe}_{1.8-x}]\text{O}_4$ ($x=0, 0.05, 0.10, 0.15, 0.20, 0.25$) were designed and prepared by a standard solid-phase method using nanoscale oxide as the raw materials. Interestingly, with an appropriate doping level, Co^{2+} ions-doped Ni–Cu–Zn ferrites can maintain relatively high soft magnetic properties, and its saturation magnetization are greatly improved. The results show that the novel Ni–Cu–Zn ferrites have better soft magnetic properties and higher saturation magnetization than pure Ni–Cu–Zn ferrites, and they have a wider range of application.

2 Experimental procedures

2.1 Synthesis

All kinds of Co-doped Ni–Cu–Zn ferrites used in this study were prepared by standard solid-phase method, their chemical formula were $[\text{Ni}_{0.6}\text{Zn}_{0.4}][\text{Cu}_{0.2}\text{Co}_x\text{Fe}_{1.8-x}]\text{O}_4$ ($x=0, 0.05, 0.10, 0.15, 0.20, 0.25$). The raw materials for preparation are nickel oxide (NiO, 99% purity), zinc oxide (ZnO, 99% purity), copper oxide (CuO, 99% purity), cobalt oxide (Co_2O_3 , 99% purity), and ferric oxide (Fe_2O_3 , 98.5% purity). All raw materials were purchased from Aladdin and Macklin. First, in order to make samples, the weighed oxide is poured into the ball mill jar, and 500 g steel ball is added with 50 ml water. The material, water, and steel ball ratio were 1:1:10. The oxide materials were further ground at a rate of 300 rpm/min for 3 h, then the mixture was placed in

a dry box and baked at 423 K for 12 h. And the dried powder was sintered at a high temperature of 1223 K for 3 h. Second, in order to make the magnetic ring, part of the powder was subjected to secondary ball milling at 300 rpm/min for 2 h, then dried in a drying oven at 393 K for 12 h, and the baked material was added to a 5 wt% polyvinyl alcohol binder for compression and the magnetic ring was sintered at 1223 K for 3 h.

2.2 Characterization

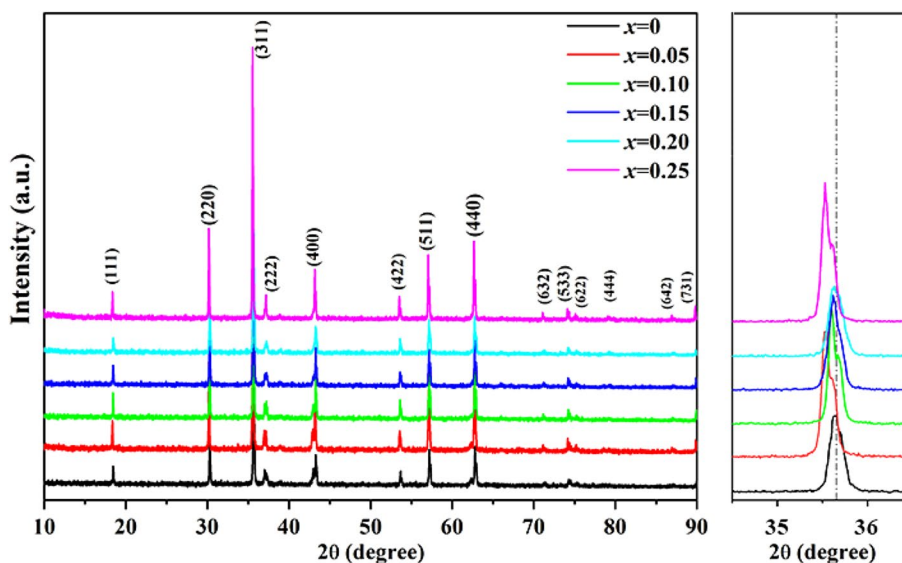
The phase of prepared samples was characterized by X-ray powder diffraction (XRD) with Cu $K\alpha$ (PHILIPS, $\lambda_{\alpha 1}=1.5406 \text{ \AA}$, $\lambda_{\alpha 2}=1.5443 \text{ \AA}$, $K_{\alpha 1}:K_{\alpha 2}=2:1$) radiation. The high resolution scanning electron microscope (SEM, Hitachi S-4800) was used to characterize the average grain size and morphology for studying the microstructure. The presence of Co^{2+} ions were detected by energy-dispersive X-Ray spectroscopy (EDX) scanning, confirming that Co^{2+} ions were doped into the Ni–Cu–Zn ferrites. The $M(H)$ curve was plotted using a quantum design superconducting quantum interferometer vibrating sample magnetometer (SQUID-VSM). The magnetic permeability and hysteresis loss were characterized by a B–H AC magnetic characteristic analyzer (Riken Denshi ACBH100K).

3 Results and discussion

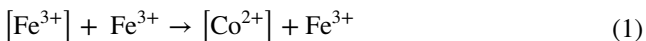
3.1 Analysis of microstructures and composition

Figure 1 shows the X-ray diffraction pattern of the $[\text{Ni}_{0.6}\text{Zn}_{0.4}][\text{Cu}_{0.2}\text{Co}_x\text{Fe}_{1.8-x}]\text{O}_4$ ($x=0, 0.05, 0.10, 0.15, 0.20, 0.25$) system. All reflection peaks of sample powders are compared to

Fig. 1 XRD patterns of $[\text{Ni}_{0.6}\text{Zn}_{0.4}][\text{Cu}_{0.2}\text{Co}_x\text{Fe}_{1.8-x}]\text{O}_4$ ($x=0, 0.05, 0.10, 0.15, 0.20, 0.25$) samples



the Ni–Zn ferrites phase of a standard PDF card (52-0277). By matching, the main peaks of all samples corresponded to the (111), (220), (311), (222), (400), (422), (511), (440), (623), (533), (622), (444), (642), and (731) crystal plane faces, the main peaks of all prepared samples are at $2\theta = 18.349^\circ, 30.136^\circ, 35.480^\circ, 37.184^\circ, 43.231^\circ, 53.310^\circ, 57.16^\circ, 62.821^\circ, 71.13^\circ, 74.11^\circ, 75.98^\circ, 79.53^\circ, 86.98^\circ, \text{ and } 89.92^\circ$ [1]. By observing the diffraction peaks of Fig. 1, it can be found that the crystal lattice has a slight expansion upon cobalt ion substitution. Through the Eq. (1):



and one Fe^{3+} is replaced by one Co^{2+} . The sum of Co^{2+} (0.0745 nm) and Fe^{3+} (0.0645 nm) radius is bigger than two Fe^{3+} (0.0645 nm) radius, relatively large cation substitution leads to lattice expansion [2]. Due to the difference in the ionic radius of the doping, it shows a significant leftward shift from the enlarged portion (within $2\theta = 35^\circ\text{--}36^\circ$) of Fig. 1 at 311 peak. Through the calculation of Bragg’s formula (2):

$$2d \cdot \sin \theta = n \cdot \lambda \tag{2}$$

where d is the lattice spacing, λ is the wavelength, θ is the diffraction angle. Co^{2+} ions occupies the A-site of the crystal structure, replacing some of the iron ions, the crystal size becomes larger, so the peak shifts to the left. The prepared samples are all crystallized in the cubic phase of the Fd-3m space group, and the Ni–Cu–Zn ferrites sample have a cubic spinel structure [3–13].

Figure 2 represents the Rietveld refined room temperature powder XRD patterns of $[\text{Ni}_{0.6}\text{Zn}_{0.4}][\text{Cu}_{0.2}\text{Co}_x\text{Fe}_{1.8-x}]\text{O}_4$ ($x = 0, 0.05, 0.10, 0.15, 0.20, 0.25$). In fact, when the value of c^2 is less than 2 and close to 1, a good refinement can be obtained. The results obtained are consistent with XRD, all samples are single phase, without any detectable secondary phase, and crystallized in a cubic structure with Fd-3m space group. The XRD data are refined by Rietveld technology, and we can get the lattice parameters of the samples. Figure 3 shows the lattice parameters (a, b and c) and unit cell volume (V) of all $\text{Ni}_{0.6}\text{Cu}_{0.2}\text{Zn}_{0.4}\text{Co}_x\text{Fe}_{1.8-x}\text{O}_4$ samples, which are calculated by the following formulae (3), (4):

$$a = d \cdot (h^2 + k^2 + l^2)^{1/2} \tag{3}$$

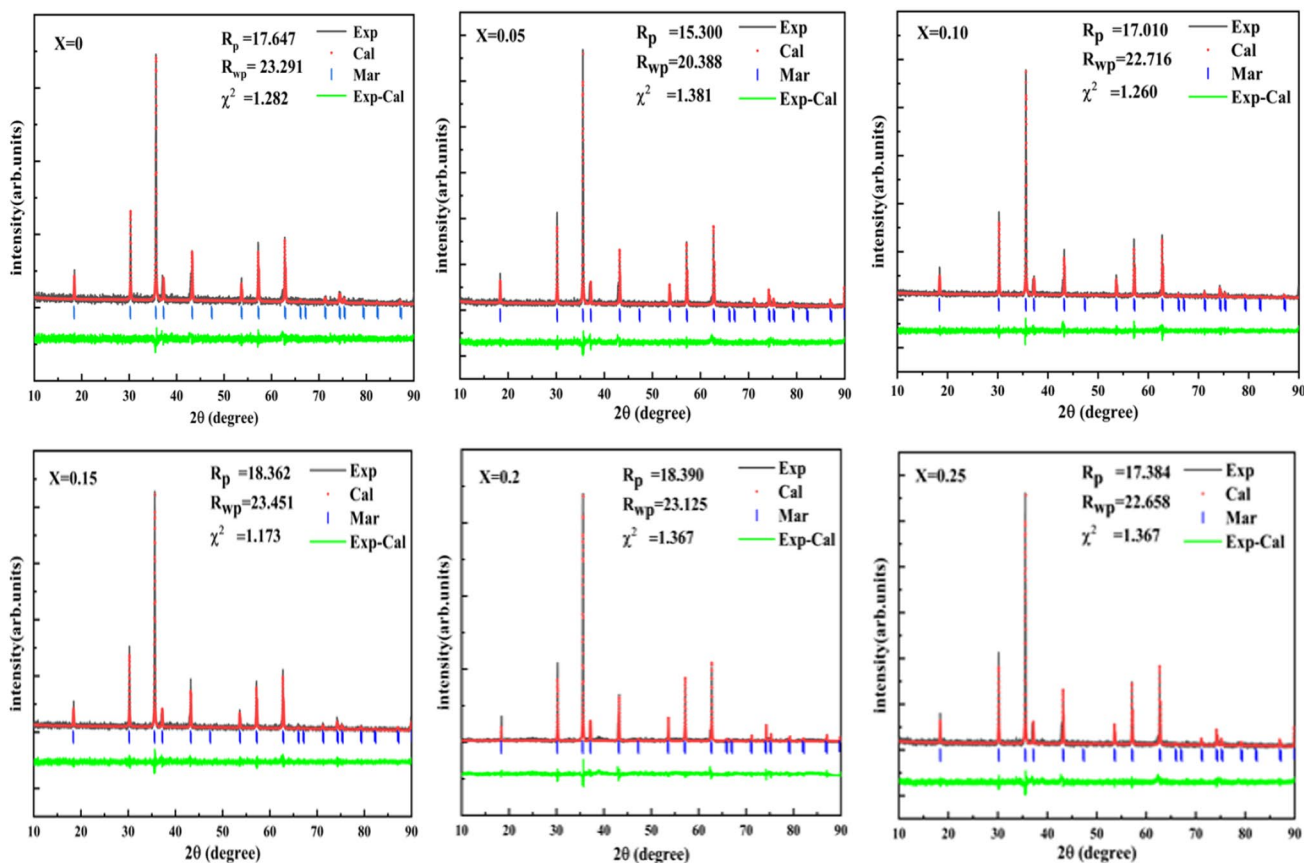


Fig. 2 Refined X-ray powder diffraction of $[\text{Ni}_{0.6}\text{Zn}_{0.4}][\text{Cu}_{0.2}\text{Co}_x\text{Fe}_{1.8-x}]\text{O}_4$ ($x = 0, 0.05, 0.10, 0.15, 0.20, 0.25$)

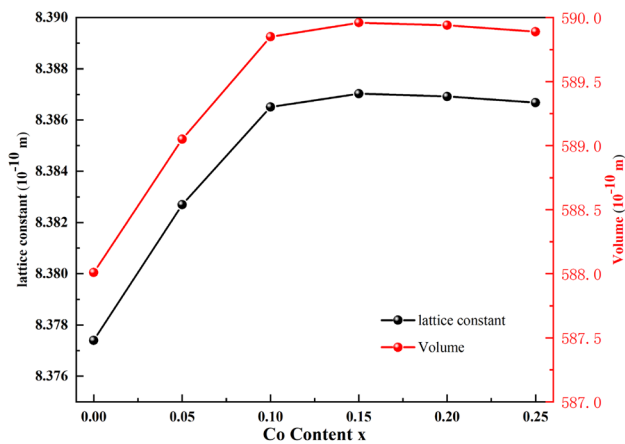


Fig. 3 Variation of lattice constant and cell volume of Co content ($x=0-0.25$)

Table 1 Fundamental structural parameters of the prepared ferrite samples

Comp. (x)	a (Å)	b (Å)	c (Å)	V (Å ³)	Density (g/cm ³)
0	8.3774	8.3774	8.3774	588.01	5.3708
0.05	8.3827	8.3827	8.3827	589.05	5.3613
0.10	8.38651	8.38651	8.38651	589.85	5.3540
0.15	8.38703	8.38703	8.38703	589.96	5.3530
0.20	8.38692	8.38692	8.38692	589.94	5.3532
0.25	8.38668	8.38668	8.38668	589.89	5.3537

$$V_{\text{cell}} = a^3 \quad (4)$$

where d is the lattices spacing, h , k and l are the Miller indices, the specific values are shown in Table 1. We can clearly find that the lattice parameters and unit cell volume show the same trend, which correlates with the results of XRD analysis.

Figure 4a–d show typical photomicrograph of $[\text{Ni}_{0.6}\text{Zn}_{0.4}][\text{Cu}_{0.2}\text{Co}_x\text{Fe}_{1.8-x}]\text{O}_4$ ($x=0, 0.05, 0.10, 0.15, 0.20, 0.25$) with different doping contents under scanning electron microscopy (SEM), and photomicrographs of these samples were taken at 10,000 times magnification. As shown, doping cobalt into the sample has a certain effect on its size and structure, which makes the sample agglomerate. The agglomeration of the powder is evident due to the magnetic dipole interaction between the powders, causing the powders to agglomerate with each other. Even if the sample is agglomerated, but all samples had a uniform grain size with a particle size ranging from 1.5 to 2.5 μm and were evenly distributed during the replacement process [1, 14]. This result echoes the above results, and the difference in ionic radius of different ions will cause a slight increase in grain size.

In order to confirm that Co^{2+} ions are doped into the Ni–Cu–Zn ferrites, the experimental samples were subjected to EDX scanning analysis, the spectrum of some samples are shown in Fig. 5. As can be seen from the figure, the samples show the peaks of pure elements of Fe, Ni, Zn, Cu, Co, and O. With the increase of cobalt element, the concentration of cobalt increases, the atomic ratio and mass ratio of cobalt also increases, confirming that cobalt is doped into Ni–Cu–Zn ferrite [1, 11, 14].

3.2 Analysis of soft magnetic performance

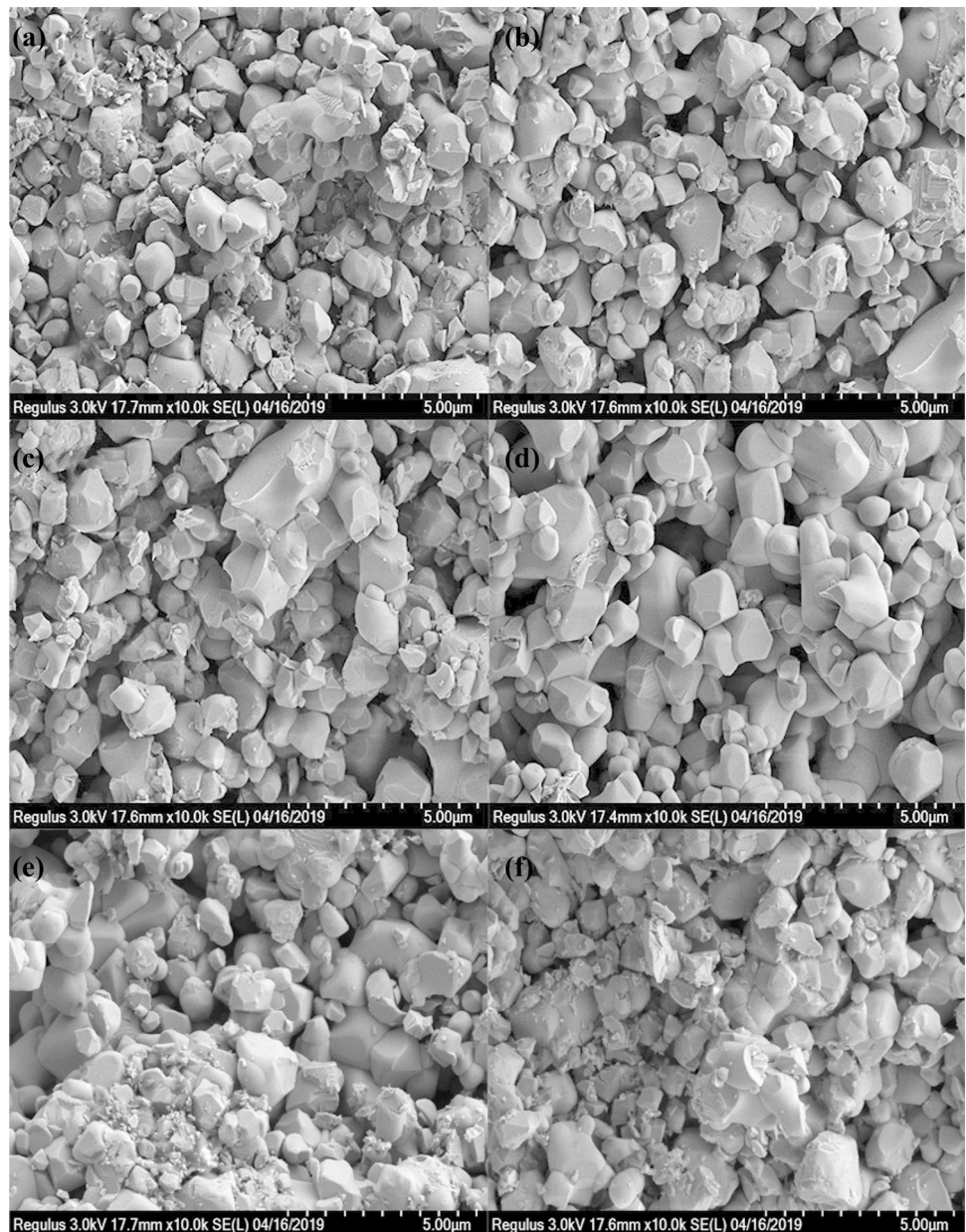
Figures 6 and 7 show hysteresis loops for all fabricated samples at 5 K and 300 K, specific data are shown in Table 2. Saturation magnetization (M_s) is the main technical parameter to characterize the magnetism of a ferromagnetic particle sample. All samples are measured using a vibrating sample magnetometer (VSM) under the condition of 300 K and 5 K, and are measured under a strong magnetic field of 30,000 oe. It can be clearly seen from Figs. 6 and 7 that the 300 K trend basically shows the same trend as 5 K. As well known, the saturation magnetization under low temperature conditions is higher than that under normal temperature conditions. When the sample is undoped with Co^{2+} , the saturation magnetization is 104.45 emu/g, and when $x=0.1$, the saturation magnetization reaches a maximum value of 118.08 emu/g. When the doping amount increases, the saturation magnetization decreases sharply, when $x=0.25$, the saturation magnetization is only 83.17 emu/g. Under 300 K conditions, when the sample is undoped with Co^{2+} , the saturation magnetization is 70.73 emu/g, and when $x=0.1$, the saturation magnetization increases continuously and reaches a maximum value of 79.12 emu/g. When the doping amount increases, the saturation magnetization decreases sharply, when $x=0.25$, the saturation magnetization is only 55.71 emu/g.

The definition of saturation magnetization is (5):

$$M_s = |M_B - M_A| \quad (5)$$

where M_B and M_A are the magnetic moments in octahedral (B) and tetrahedral (A) sites [5]. The O^{2-} radius in the spinel ferrite is larger, and an O^{2-} ion layer is deposited around the lattice structure, but the metal ions have a small radius and are filled in the dense O^{2-} ion layer gap. The unit cell structure of ferrite consists of a tetrahedral structure and an octahedral structure. The octahedral structure forms 32 B-sites, and the tetrahedral structure forms 64 A-sites, but in fact only fills 8 A-sites and 16 B-sites. A large number of literatures have confirmed that Zn^{2+} occupies the A-site, Ni^{2+} occupies the B-site, and Fe^{3+} simultaneously occupies the A-site and B-site [5, 17]. In the spinel ferrite, each ion at A-site has 12 B-site ions as the nearest ion, the concentration

Fig. 4 SEM micrographs of sintered $[\text{Ni}_{0.6}\text{Zn}_{0.4}][\text{Cu}_{0.2}\text{Co}_x\text{Fe}_{1.8-x}]\text{O}_4$ ferrite with **a** $x=0.00$, **b** $x=0.05$, **c** $x=0.10$, **d** $x=0.15$, **e** $x=0.20$ and **f** $x=0.25$. The white bar indicates 5 μm



of the A-site is lower than the B-site. First, the Co^{2+} ions preferentially occupy the A-site, which replace the Fe^{3+} ions at the A-site, and the magnetic moment of Ni^{2+} ion is equal to $2 \mu_{\text{B}}$, Cu^{2+} ion is $1 \mu_{\text{B}}$, Co^{2+} ion is $3 \mu_{\text{B}}$, Zn^{2+} ion is $0 \mu_{\text{B}}$ and Fe^{3+} is $5 \mu_{\text{B}}$ [18–23]. Obviously, the magnetic moment of Co^{2+} ion is lower than the magnetic moment of Fe^{3+} ion, the magnetic moment at the A position is reduced, and the magnetic moment direction is parallel and opposite. According to the principle of super-exchange, the A–B site’s super-exchange effect is enhanced, but the A–A site’s super-exchange effect is weakened and the M_s is increased [10, 24]. When the doping amount of cobalt ions is greater than 0.1, Co^{2+} ions begin to occupy the B-site, replacing the Fe^{3+} ions at the B-site [18–23]. Since the magnetic

moments of Co^{2+} ions are much lower than the Fe^{3+} ions, the magnetic moment at the B-site is greatly reduced, and the super-exchange effect at the B–B site is also weakened, which causes a decrease in M_s [24–26].

Figure 8 shows the relationship between the real permeability of ferrite and frequency. According to Refs. [5, 19], the real permeability is related to spin rotation and domain wall motion. The specific calculation formula is as follows (6), (7), (8):

$$\mu' = 1 + \mu_w + \mu_{\text{spin}} \quad (6)$$

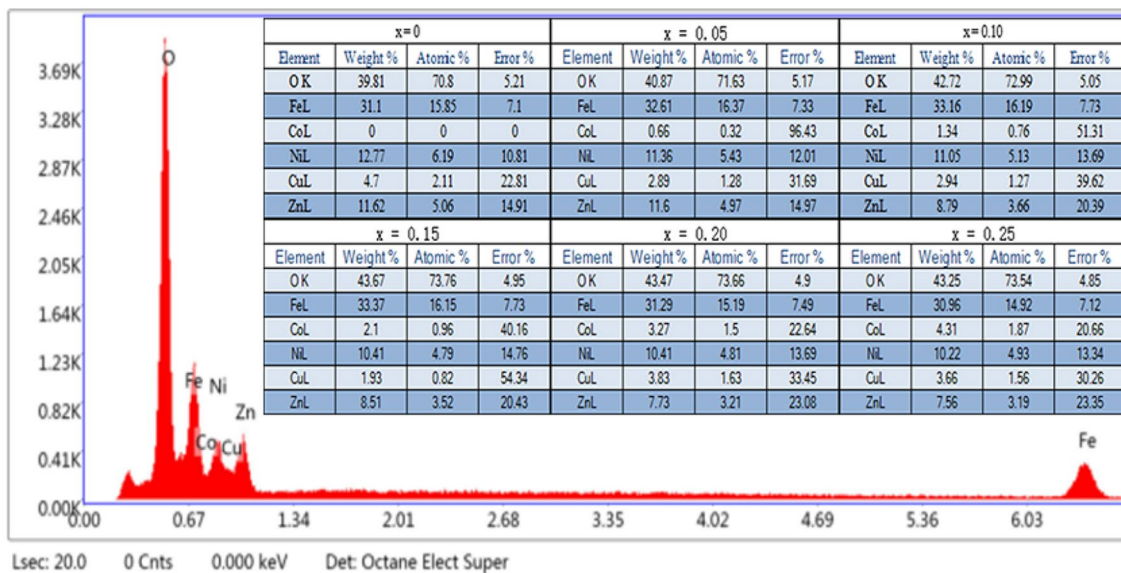


Fig. 5 EDX spectrum of [Ni_{0.6}Zn_{0.4}][Cu_{0.2}Co_xFe_{1.8-x}]O₄ (x = 0, 0.05, 0.10, 0.15, 0.20, 0.25) samples

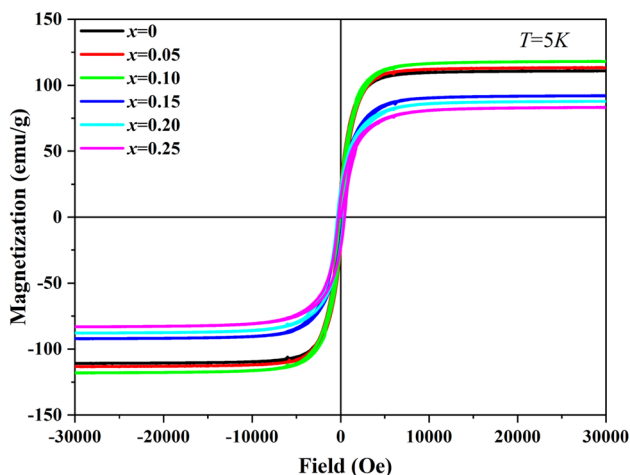


Fig. 6 Magnetic hysteresis loops of [Ni_{0.6}Zn_{0.4}][Cu_{0.2}Co_xFe_{1.8-x}]O₄ (x = 0, 0.05, 0.10, 0.15, 0.20, 0.25) system at 5 K

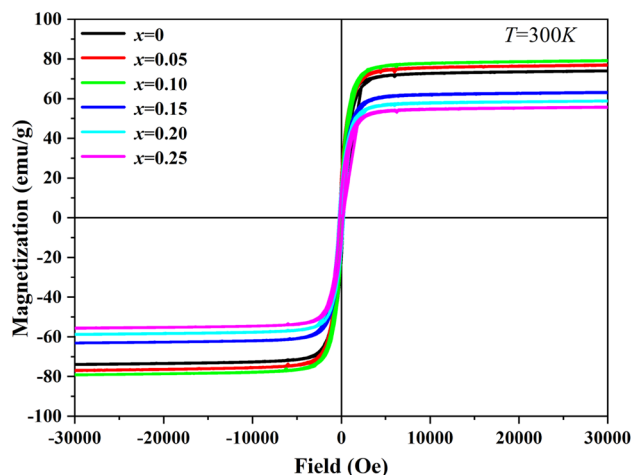


Fig. 7 Magnetic hysteresis loops of [Ni_{0.6}Zn_{0.4}][Cu_{0.2}Co_xFe_{1.8-x}]O₄ (x = 0, 0.05, 0.10, 0.15, 0.20, 0.25) system at 300 K

$$\mu_w = \frac{2\pi M_s^2 D}{4\gamma} \tag{7}$$

$$\mu_{spin} = \frac{2\pi M_s^2}{K} \tag{8}$$

where μ_w is the domain wall susceptibility, μ_{spin} is the intrinsic rotational susceptibility, M_s is the saturation magnetization, D is the mean size of ferrite grains, γ is the domain wall energy, and K is the magnetocrystalline anisotropy constant [5, 27]. In this study, since the content of Co²⁺ ions is relatively low, and the value of γ is determined by

Table 2 Saturation magnetization and hysteresis loss of the prepared ferrite samples

Comp. (x)	M_s (5 K)	M_s (300 K)	P_{cv} (100 kHz)
0	104.45	70.73	1.192
0.05	113.40	77.02	1.713
0.10	118.08	79.12	1.44
0.15	92.11	63.12	11.99
0.20	87.80	58.84	18.51
0.25	83.17	55.71	22.61

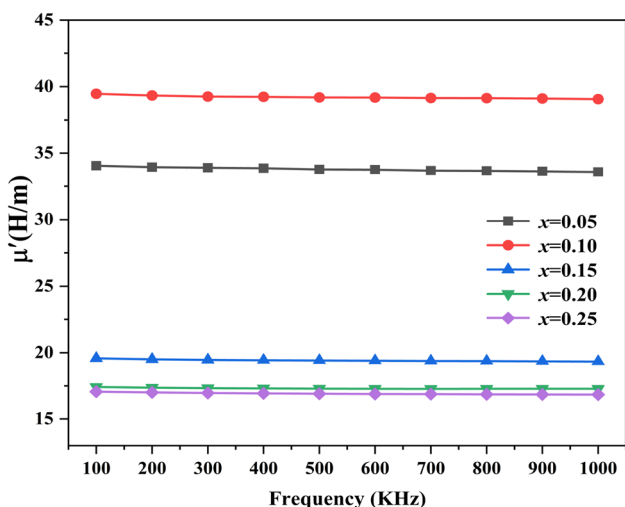


Fig. 8 Frequency dependence of the real permeability of the as-acquired $[\text{Ni}_{0.6}\text{Zn}_{0.4}][\text{Cu}_{0.2}\text{Co}_x\text{Fe}_{1.8-x}]\text{O}_4$ ($x=0.05, 0.10, 0.15, 0.20, 0.25$) samples

the type and concentration of the dopant, the value of γ can be regarded as a constant [5, 27]. Observing Eqs. (6), (7), (8), the value of the real permeability is mainly determined by the values of M_s , D and K , in addition, doping Co^{2+} ions can significantly increase the K value of the sample [5]. In case of ferrites with Co doping < 0.1 , the values of M_s and D are greatly increased, and the increasing trend is much larger than the increasing trend of K value, so the real magnetic permeability is significantly increased. In case of ferrites with Co doping > 0.1 , the value of magnetocrystalline anisotropy constant (K) of Co^{2+} ion is positive, while those of Ni–Cu–Zn ferrites are negative, using compensation of negative and positive value can make $K \rightarrow 0$, The value of D does not change much, but the value of M_s is drastically lowered, so the value of the real magnetic permeability is lowered [16].

The P_{cv} of ferrite materials can be divided into hysteresis loss (P_h), eddy current loss (P_e), and residual loss (P_r). The hysteresis loss of Ni–Cu–Zn ferrite can be regarded as the algebraic sum of various losses only in the case of low frequency and weak magnetic field. At the same time, according to the formula (9) of the hysteresis loss:

$$p = \frac{4\mu_0 b}{3} H_m^3 f \tag{9}$$

where μ_0 is vacuum permeability, b is Rayleigh constant, H_m is magnetic field strength, f is the operating frequency. Figure 9 shows the relationship between hysteresis loss and frequency at a magnetic flux density of 5 mT. It can be seen from the figure that while the frequency is increasing, the overall trend of hysteresis loss is also increasing. When

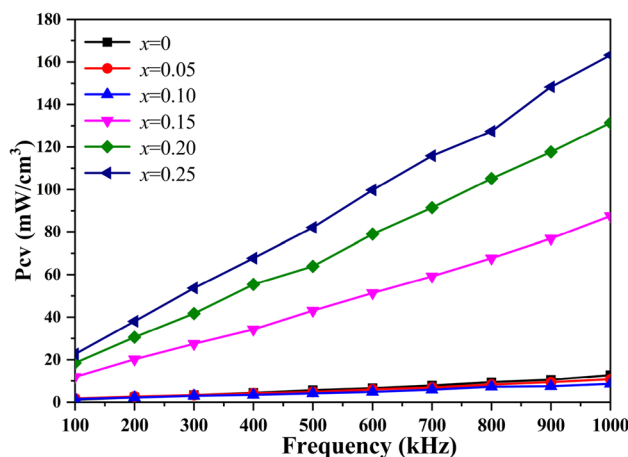


Fig. 9 Relationship between power loss and frequency at 5 mT

$x < 0.1$, the hysteresis loss at the same frequency decreases with the increase of cobalt doping amount, and by comparing with the value of undoped sample, the average decrease is 21.88%. When $x > 0.1$, the hysteresis loss of the sample increases sharply with the increase of cobalt doping amount, and by comparing with the value of undoped sample, the average increase is 17.74 times. As a typical ferromagnetic substance, cobalt is used to increase the magnetic properties of the sample and reduce the hysteresis loss when it is doped at a low content [26–33]. Since the doping amount is too high, some impurities enter the inside of the crystal, which destroy the crystal structure of the material, and the hysteresis loss of the sample also decreases [34, 35].

4 Conclusion

This paper demonstrates that Co-doped Ni–Cu–Zn ferrites can change its nanostructure and thus change the magnetic properties of Ni–Cu–Zn ferrites. XRD, SEM, and EDS results show that the microstructure of the sample does change with the incorporation of Co^{2+} ions, and the lattice constant and average lattice size are increased continuously. With the magnetic property data obtained by the AC magnetic characteristic analyzer and VSM, as the cobalt doping amount increases, the saturation magnetization and magnetic permeability first increase and then decrease, and the hysteresis loss decreases first and then increases. The experimental results show that when the doping amount of cobalt is 0.1, the sample achieves the best magnetic properties. The maximum value of saturation magnetization at room temperature is 79.12 emu/g, the maximum value of saturation magnetization at low temperature is 118.08 emu/g, the maximum value of magnetic permeability is 39.47 H/m, and the lowest value of hysteresis loss is 1.192 kw/cm³. This study shows that the Co-doped-Ni–Cu–Zn ferrites have changes in their magnetic

properties, and the obtained samples are with high saturation magnetization, low hysteresis loss, and high magnetic permeability, which improves the application range of the sample.

Acknowledgements This work was supported by the National Natural Science Foundation of China (Grant Nos. 51872004, 51802002), Education Department of Anhui Province (Grant Nos. KJ2013B293, KJ2018A0039).

References

1. D.L. Zhao, Q. Lv, Z.M. Shen, Fabrication and microwave absorbing properties of Ni–Zn spinel ferrites. *J. Alloy. Compd.* **480**(2), 634–638 (2009)
2. S.J. Feng, J. Li, S.G. Huang, Magnetic hysteresis loss crossover in $\text{Ni}_{0.4}\text{Zn}_{0.6}\text{Fe}_{1.95}\text{Ti}_{0.05}\text{O}_4$ ferrite. *J. Alloy. Compd.* **660**, 398–401 (2016)
3. T. Nakamura, Low-temperature sintering of NiZnCu ferrite and its permeability spectra. *J. Magn. Magn. Mater.* **168**(3), 285–291 (1997)
4. M. Fujimoto, Inner stress induced by Cu metal precipitation at grain boundaries in low-temperature-fired Ni–Zn–Cu ferrite. *J. Am. Ceram. Soc.* **77**(11), 2873–2878 (1994)
5. P. Yang, Z.Q. Liu, H.B. Qi, High-performance inductive couplers based on novel Ce^{3+} and Co^{2+} ions co-doped Ni–Zn ferrites. *Ceram. Int.* **45**(11), 13685–13691 (2019)
6. R.C. Kambale, N.R. Adhate, B.K. Chougule, Magnetic and dielectric properties of mixed spinel Ni–Zn ferrites synthesized by citrate–nitrate combustion method. *J. Alloy. Compd.* **491**(1–2), 372–377 (2010)
7. T. Nakamura, Y. Okano, S. Miura, Interfacial diffusion between Ni–Zn–Cu ferrite and Ag during sintering. *J. Mater. Sci.* **33**(4), 1091–1094 (1998)
8. S.E. Shirsath, R.H. Kadam, S.M. Patange, M.L. Mane, A. Ghasemi, A. Morisako, *Appl. Phys. Lett.* **100**(4), 42407 (2012)
9. L. Li, L. Peng, Y. Li et al., Structure and magnetic properties of Co-substituted NiZn ferrite thin films synthesized by the sol–gel process. *J. Magn. Magn. Mater.* **324**(1), 60–62 (2012)
10. X. Pan, A. Sun, Y. Han, Structural and magnetic properties of Bi^{3+} ion doped Ni–Cu–Co nano ferrites prepared by sol–gel auto combustion method. *J. Mater. Sci.* **30**(5), 4644–4657 (2019)
11. M.P. Reddy, W. Madhuri, N.R. Reddy, Influence of copper substitution on magnetic and electrical properties of MgCuZn ferrite prepared by microwave sintering method. *Mater. Sci. Eng. C* **30**(8), 1094–1099 (2010)
12. H.B. Wang, J.H. Liu, W.F. Li, Structural, dynamic magnetic and dielectric properties of $\text{Ni}_{0.15}\text{Cu}_{0.2}\text{Zn}_{0.65}\text{Fe}_2\text{O}_4$ ferrite produced by NaOH co-precipitation method. *J. Alloy. Compd.* **461**(1), 373–377 (2008)
13. L. Néel, Magnetic properties of ferrites: ferrimagnetism and antiferromagnetism. *Ann. Phys.* **3**, 137–198 (1948)
14. G.D. Tang, D.H. Ji, Y.X. Yao, S.P. Liu, Z.Z. Li, W.H. Qi, Q.J. Han, X. Hou, D.L. Hou, Quantum-mechanical method for estimating ion distributions in spinel ferrites. *Appl. Phys. Lett.* **98**, 072511 (2011)
15. Y.M. Kwon, M.Y. Lee, M. Mustaqima, C. Liu, B.W. Lee, Structural and magnetic properties of $\text{Ni}_{0.6}\text{Zn}_{0.4}\text{Fe}_2\text{O}_4$ ferrite prepared by solid state reaction and sol–gel. *J. Magn. Magn. Mater.* **19**, 64–67 (2014)
16. J. Jadhav, S. Biswas, A.K. Yadav, S.N. Jha, D. Bhattacharyya, Structural and magnetic properties of nanocrystalline NiZn ferrites: in the context of cationic distribution. *J. Alloys Compd.* **696**, 28–41 (2017)
17. N. Singh, A. Agarwal, S. Sanghi, Effect of magnesium substitution on dielectric and magnetic properties of Ni–Zn ferrite. *Phys. B* **406**(3), 687–692 (2011)
18. R. Kumar, H. Kumar, M. Kumar, Enhanced saturation magnetization in cobalt doped Ni–Zn ferrite nanoparticles. *J. Supercond. Nov. Magn.* **28**(12), 3557–3564 (2015)
19. M. Veverka, Z. Jirak, O. Kaman, K. Knizek, M. Marysko, E. Pollert, K. Zaveta, A. Lancok, M. Dlouha, S. Vratislav, Distribution of cations in nanosize and bulk Co–Zn ferrites. *Nanotechnology* **22**, 345701 (2011)
20. E.J. Choi, Y.K. Ahn, K.C. Song, D.H. An, B.G. Lee, K.U. Kang, Cation distribution and spin-canted structure in cobalt ferrite particles from a cobalt–iron hydroxide carbonate complex. *J. Korean Phys. Soc.* **44**, 1518–1520 (2004)
21. M.K. Fayek, A.A. Bahgat, Y.M. Abbas, L. Moberg, Neutron diffraction and Mossbauer effect study on a cobalt substituted zinc ferrite. *J. Phys. C* **15**, 2509–2518 (1982)
22. G.A. Sawatzky, F. Van Der Woude, A.H. Morrish, Mössbauer study of several ferrimagnetic spinels. *Phys. Rev.* **187**, 747 (1969)
23. A.M. Kumar, P.A. Rao, M.C. Varma, G.S. Choudary, K.H. Rao, Cation distribution in $\text{Co}_{0.7}\text{Me}_{0.3}\text{Fe}_2\text{O}_4$. *J. Mod. Phys.* **2**, 1083 (2011)
24. J.Y. Hu, X.S. Liu, X.C. Kan, Characterization of texture and magnetic properties of $\text{Ni}_{0.5}\text{Zn}_{0.5}\text{Ti}_x\text{Fe}_{2-x}\text{O}_4$ spinel ferrites. *J. Magn. Magn. Mater.* **489**, 165411 (2019)
25. A.R. Das, V.S. Ananthan, D.C. Khan, Lattice parameter variation and magnetization studies on titanium-, zirconium-, and tin-substituted nickel–zinc ferrites. *J. Appl. Phys.* **57**(8), 4189–4191 (1985)
26. D.C. Khan, M. Misra, Magnetic, Mössbauer and electrical properties of Ti-substituted $\text{Ni}_{0.3}\text{Zn}_{0.7}\text{Fe}_2\text{O}_4$. *Bull. Mater. Sci.* **7**(3–4), 253–270 (1985)
27. K.K. Bharathi, G. Markandeyulu, C.V. Ramana, Structural, magnetic, electrical, and magnetoelectric properties of Sm- and Ho-substituted nickel ferrites. *J. Phys. Chem. C* **115**(2), 554–560 (2010)
28. D. Hu, F. Zhao, L. Miao, Magnetic properties and microstructures of a Ni–Zn ferrite ceramics co-doped with V_2O_5 and MnCO_3 . *Ceram. Int.* **45**(8), 10028–10034 (2019)
29. S.S. Kim, D.H. Han, S.B. Cho, Microwave absorbing properties of sintered Ni–Zn ferrite. *IEEE Trans. Magn.* **30**(6), 4554–4556 (1994)
30. F. Gen, E. Turhan, H. Kavaz, Magnetic and microwave absorption properties of $\text{Ni}_x\text{Zn}_{0.9-x}\text{Mn}_{0.1}\text{Fe}_2\text{O}_4$ prepared by boron addition. *J. Supercond. Nov. Magn.* **28**(3), 1047–1050 (2015)
31. S. Modak, M. Ammar, F. Mazaleyrat, XRD, HRTEM and magnetic properties of mixed spinel nanocrystalline Ni–Zn–Cu-ferrite. *J. Alloy. Compd.* **473**(1), 15–19 (2009)
32. P. Priyadharsini, A. Pradeep, P.S. Rao, Structural, spectroscopic and magnetic study of nanocrystalline Ni–Zn ferrites. *Mater. Chem. Phys.* **116**(1), 207–213 (2009)
33. H. Su, X. Tang, H. Zhang, Influences of Bi_2O_3 additive on the microstructure, permeability, and power loss characteristics of Ni–Zn ferrites. *J. Magn. Magn. Mater.* **321**(19), 3183–3186 (2009)
34. S.V. Trukhanov, Magnetic and magnetotransport properties of $\text{La}_{1-x}\text{Ba}_x\text{MnO}_{3-x/2}$ perovskite manganites. *J. Mater. Chem.* **13**(2), 347–352 (2003)
35. V.D. Doroshev, V.A. Borodin, V.I. Kamenev, Self-doped lanthanum manganites as a phase-separated system: transformation of magnetic, resonance, and transport properties with doping and hydrostatic compression. *J. Appl. Phys.* **104**(9), 093909 (2008)

Publisher's Note Springer Nature remains neutral with regard to jurisdictional claims in published maps and institutional affiliations.